PNAS Nexus, 2024, 3, pgae275
https://doi.org/10.1093/pnasnexus/pgae275
Advance access publication 20 July 2024
Research Report

Glutamatergic signaling from melanin-concentrating hormone-producing neurons: A requirement for memory regulation, but not for metabolism control

Xuan Thang Pham [a,b,c,d], Yoshifumi Abe [e], Yasutaka Mukai [a,b,f], Daisuke Ono [a,b], Kenji F. Tanaka [e], Yu Ohmura [g], Hiroaki Wake [c] and Akihiro Yamanaka [e,g,h,*]

[a]Department of Neuroscience II, Research Institute of Environmental Medicine, Nagoya University, Nagoya 464-8601, Japan
[b]Department of Neural Regulation, Nagoya University Graduate School of Medicine, Nagoya 466-8550, Japan
[c]Department of Anatomy and Molecular Cell Biology, Nagoya University Graduate School of Medicine, Nagoya 466-8550, Japan
[d]Department of Psychiatry, Hanoi Medical University, Hanoi 100000, Vietnam
[e]Division of Brain Sciences, Institute for Advanced Medical Research, Keio University School of Medicine, Tokyo 160-8582, Japan
[f]Japan Society for the Promotion of Science, Tokyo 102-0083, Japan
[g]Chinese Institute for Brain Research, Beijing (CIBR), Beijing 102206, China
[h]National Institute for Physiological Sciences, National Institutes of Natural Sciences, Aichi 444-8585, Japan
*To whom correspondence should be addressed: Email: yamank@cibr.ac.cn
Edited By Patrick Stover

Abstract

Melanin-concentrating hormone-producing neurons (MCH neurons), found mainly in the lateral hypothalamus and surrounding areas, play essential roles in various brain functions, including sleep and wakefulness, reward, metabolism, learning, and memory. These neurons coexpress several neurotransmitters and act as glutamatergic neurons. The contribution of glutamate from MCH neurons to memory- and metabolism-related functions has not been fully investigated. In a mouse model, we conditionally knocked out *Slc17a6* gene, which encodes for vesicular glutamate transporter 2 (vGlut2), in the MCH neurons exclusively by using two different methods: the Cre recombinase/loxP system and in vivo genome editing using CRISPR/Cas9. Then, we evaluated several aspects of memory and measured metabolic rates using indirect calorimetry. We found that mice with MCH neuron-exclusive vGlut2 ablation had higher discrimination ratios between novel and familiar stimuli for novel object recognition, object location, and three-chamber tests. In contrast, there was no significant change in body weight, food intake, oxygen consumption, respiratory quotient, or locomotor activity. These findings suggest that glutamatergic signaling from MCH neurons is required to regulate memory, but its role in regulating metabolic rate is negligible.

Keywords: melanin-concentrating hormone (MCH), glutamate, vglut2, memory, metabolic regulation

Significance Statement

Melanin-concentrating hormone-producing neurons (MCH neurons) regulate various vital physiological processes. In addition to the MCH peptide, these neurons coexpress several other neurotransmitters, which are involved in complex molecular control of their functions. We investigated the role of glutamatergic signaling from MCH neurons in memory and metabolism. We found that mice lacking vesicular glutamate transporter 2 (vGlut2) showed improvements in a variety of memory facets. However, this signaling pathway seems to have a negligible effect on metabolic rate. These findings highlight the sophistication of MCH neurons in utilizing their neurotransmitters to function, suggesting that further deeper investigations are warranted to reveal the contribution of these neurons to physiological and pathological states from a molecular perspective. This approach may suggest potential treatments for some amnestic conditions.

Introduction

Melanin-concentrating hormone (MCH) is a cyclic 19-amino-acid peptide, and MCH-producing neurons (MCH neurons) are specialized cells located primarily in the lateral hypothalamic area (LHA) and surrounding areas of the brain such as the zona incerta (1). With extensive projections throughout various brain areas, MCH neurons are part of the neural network that regulates many physiological processes, including energy homeostasis (2–4), sleep

Competing Interest: The authors declare no competing interests.
Received: August 11, 2023. **Accepted:** June 29, 2024

and wakefulness (5–7), reward and reinforcement feeding (8), memory, and learning (9).

There has been growing interest in elucidating the roles of MCH neurons and their neurotransmitters, including neuropeptides, in learning and memory. We reported that after MCH neuronal ablation, mice showed improved hippocampus-dependent memory. In addition, using optogenetics and chemogenetics, the activation of MCH neurons resulted in impaired memory, and their inhibition improved it (10). MCH neurons can be classified into three subpopulations based on their sleep and wakefulness-dependent activity, revealing that rapid eye movement (REM)-sleep-active MCH neurons are exclusively related to memory regulation. However, from the molecular perspective of MCH neurons, the role of MCH in memory has been inconsistent across studies. On the one hand, MCH itself may enhance memory. Infusing MCH into the hippocampus and amygdala increased the time latency or reversed the amnesic effect induced by a nitric oxide synthase inhibitor in a one-trial step-down inhibitory avoidance test in rats (11, 12), and MCH administration into the nasal cavity restored memory in mouse models of memory impairment and Alzheimer's disease (13). On the other hand, Ruiz et al. showed that acute intrahippocampal administration of MCH impaired memory consolidation in mice in a novel object recognition (NOR) test (14). Studies have also investigated MCH signaling by intervening in its receptors. In rodents, MCH receptor 1 (MCHR1) functions as the only MCH receptor (15), and MCHR1-knockout (MCHR1-KO) mice showed memory impairment in an inhibitory avoidance test, supporting the hypothesis that MCH improves memory (16).

The role of MCH neurons in regulating energy homeostasis has been emphasized in previous articles, which have reported that MCH neuronal activity promotes energy conservation and the accumulation of food intake. Overexpression of MCH in transgenic mice leads to obesity and insulin resistance (17). After MCH neuronal ablation, mice exhibit increased caloric expenditure and reduced fat weight (18). In addition, while acute or chronic intracerebroventricular administration of MCH causes hyperphagia and reduces energy expenditure (19, 20), knocking out either MCH or MCHR1 increases energy expenditure in mouse models (21).

Many studies have focused mainly on the scope of MCH transmission and MCH neurons in the functions mentioned above. However, the other molecular mechanisms by which MCH neurons regulate memory and energy metabolism are poorly understood. Other neuropeptides, including cocaine- and amphetamine-regulated transcript (CART), nesfatin 1, and vascular endothelial growth factor A (VEGF-A), are also expressed in and released from MCH neurons (22–24). Additionally, nearly all MCH neurons express vesicular glutamate transporter 2 (vGlut2), a marker of glutamatergic neurons (25–27), but most MCH neurons do not express the vesicular γ-aminobutyric acid (GABA) transporter, a marker of GABA neurons (25, 26). This pattern of expression suggests that MCH neurons are glutamatergic despite contrary evidence (28). Photoactivation of channelrhodopsin-2-expressing MCH neurons inhibits the activity of their densely projected areas, such as the lateral septum, by evoking monosynaptic glutamate release, which subsequently induces the secondary release of GABA in local microcircuits (26). Using the same method to activate MCH neurons decreases hippocampal pyramidal neuronal activity and impairs hippocampus-dependent memory (10). Glutamatergic signaling from MCH neurons is reported to play a role in anxiety-like behaviors, diurnal variability in REM sleep (29, 30), and metabolic rate, although the evidence to date remains controversial (27, 29). Thus, we believe that glutamate may play a role in or support MCH in MCH neuron-mediated functions, including memory and energy metabolism.

To elucidate the role of glutamate released by MCH neurons, we performed conditional knockout (cKO) *Slc17a6* gene (vGlut2 cKO) exclusively in MCH neurons by using two different methods: a Cre recombinase (Cre)/loxP system and by in vivo genome editing with CRISPR/Cas9. In a mouse model, our results showed that vGlut2 cKO in MCH neurons consistently improved the discrimination ratio of the mice in several memory recognition tests but did not significantly affect their metabolic rate. These results also suggest that glutamate is an essential neurotransmitter involved in memory regulation by MCH neurons but has a negligible role in controlling metabolism.

Results

Prenatal vGlut2 cKO in MCH neurons improves the ability of mice to recognize novel objects

We first examined whether glutamate released from MCH neurons plays a role in memory performance. To test this hypothesis, we evaluated the effect of selective vGlut2 cKO on MCH neurons in a NOR test using three bigenic mice: *Pmch-Cre;Slc17a6*$^{+/+}$, *Pmch-Cre;Slc17a6*$^{flox/+}$, and *Pmch-Cre;Slc17a6*$^{flox/flox}$ (Fig. 1A). Several methods were used to confirm the success of vGlut2 cKO in MCH mice. First, we performed genotyping to detect the excised *Slc17a6* sequence in the LHA of *Pmch-Cre;Slc17a6*$^{flox/+}$ and *Pmch-Cre;Slc17a6*$^{flox/flox}$ mice. Initially, the *Slc17a6*^{flox} genotype was checked by PCR using mouse tail samples and primer pair 1, in which the forward and reverse primers are located upstream and downstream of the second loxP site, respectively (Fig. 1B). Then, the mice were euthanized and their brains were fixed in 10% formalin. Theoretically, where Cre is expressed, exon 2 of the *Slc17a6*^{flox} allele, flanked between the two loxP sites, is excised. We used nested PCR to increase the specificity of our PCR amplification (Fig. 1C). The shared forward primer is located upstream of the first loxP site, and the two reverse primers are located downstream from the second loxP site. The product from the first PCR round was used as the DNA template in the second round. We carefully excised the LHA from mouse brain slices to include as many MCH neurons as possible. Cortical and hippocampal areas were used as controls (Fig. 1D, left). PCR and electrophoresis yielded 536 and 508 bp bands in the first and second rounds, respectively, which were detected exclusively in the LHA of *Pmch-Cre;Slc17a6*$^{flox/+}$ and *Pmch-Cre;Slc17a6*$^{flox/flox}$ mice, but not in other brain areas or in *Pmch-Cre;Slc17a6*$^{+/+}$ mice (Fig. 1D, right). After subcloning, these PCR products were sequenced, and the results confirmed that the detected bands were amplicons of the excised *Slc17a6*^{flox} allele. This finding suggests that *Slc17a6* gene was knocked out in some neuronal populations of the LHA. The amplicons of *Slc17a6*$^{+}$ and intact *Slc17a6*^{flox} were not detected on agarose gels, which could be explained by the limited ability to amplify large amplicons (>2 kb) from crude genomic DNA. Second, we performed immunohistochemistry (IHC) to confirm the lack of vGlut2 in the axons of MCH neurons. *Pmch-Cre;Rosa26*$^{LSL\text{-}tdTomato}$*;Slc17a6*$^{+/+}$ mice were used as a control group to quantify the vGlut2 expression in the axons of MCH neurons (Fig. S1A, left column). In this group, 94.56% of MCH-neuron axons observed in the CA1 area of the hippocampus (87/92 axons from 3 mice) were positive for vGlut2 (Fig. S1B). To visualize the axons of MCH neurons in *Pmch-Cre;Slc17a6*$^{flox/flox}$ mice, adeno-associated virus (AAV)-CAG-FLEX-EGFP was injected into the LHA. None of the MCH-neuron axons in the CA1 region coexpressed vGlut2 (0/40 axons, from 3 mice; Fig. S1A, middle column, and B). These data indicate that the *Pmch-Cre;Slc17a6*$^{flox/flox}$ mice exclusively lacked vGlut2 in MCH neurons.

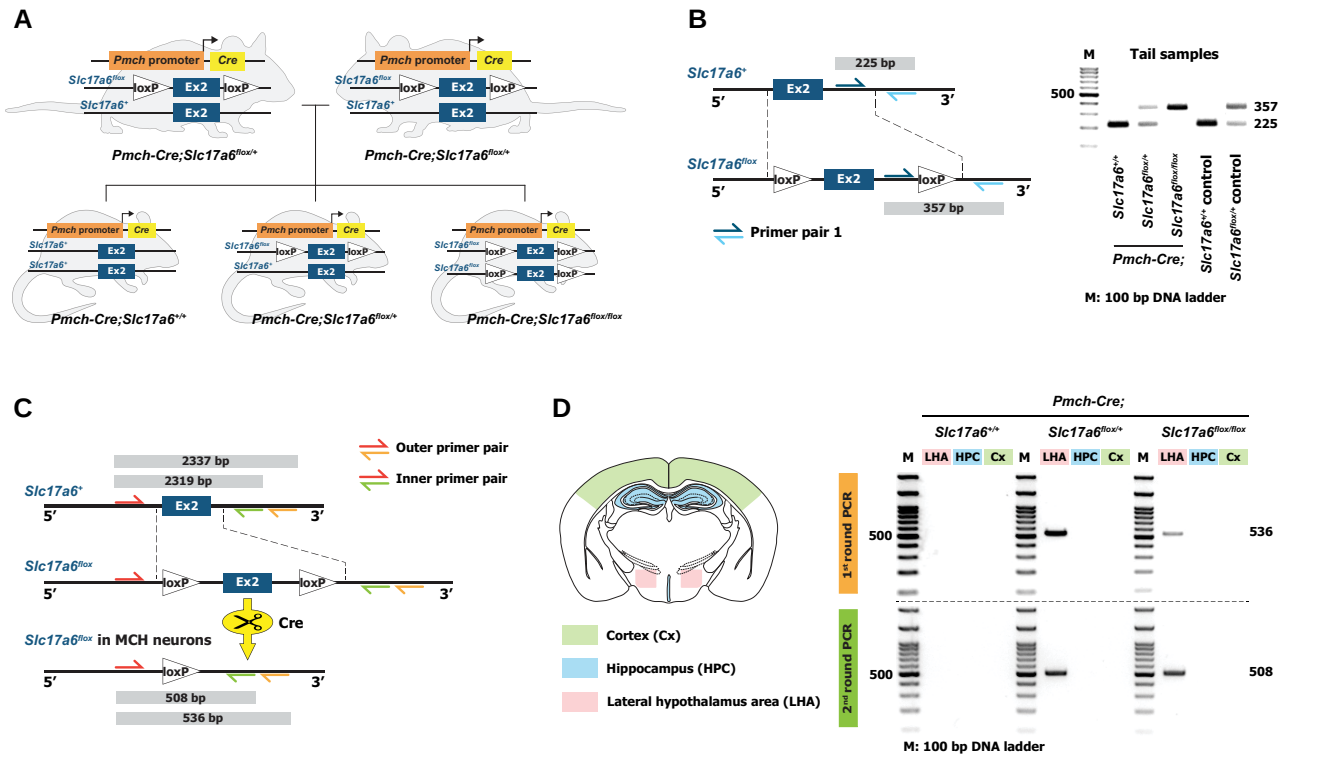

Fig. 1. Generation and validation of vGlut2 cKO in MCH neurons in mice. A) Generation of *Pmch-Cre;Slc17a6*$^{+/+}$, *Pmch-Cre;Slc17a6*$^{flox/+}$, and *Pmch-Cre;Slc17a6*$^{flox/flox}$ bigenic mice. *Slc17a6*$^{+}$ represents the wild-type *Slc17a6* allele, and *Slc17a6*^{flox} represents the *Slc17a6* allele in which exon 2 is flanked by two loxP sites. B–D) Workflow confirming vGlut2 cKO in MCH neurons using PCR genotyping. B) Genotyping using mousetail tip samples. The position of primer pair 1 is shown on the left, and the gel electrophoresis results are shown on the right. C, D) Genotyping using brain slices. C) The positions of the outer and inner primer pairs used for nested PCR and the lengths of the resulting amplicons. In MCH neurons, exon 2 of the *Slc17a6*^{flox} allele was excised by Cre between the two loxP sites (lowest panel). D) Schematic of the different brain areas (cortex, hippocampus, and LHA) from which tissue slices were obtained (left) and the electrophoresis results (right). The first-round PCR product was used as the DNA template for the second PCR round. bp: base pair.

Next, we tested the mouse memory performance in a NOR test. In this test, after 10 min of exploring two identical objects (phase 1, encoding period), the mice were kept in a home cage for 1.5 h. They were then allowed to explore the same environment where one of the identical objects was replaced by a different object (phase 2, retrieval period; Fig. 2A). All mouse genotypes showed an equal preference for the two similar objects and a longer exploration time for the novel object than for the familiar object (Fig. 2B). Interestingly, *Pmch-Cre;Slc17a6*$^{flox/flox}$ mice had a significantly higher discrimination ratio than that of *Pmch-Cre;Slc17a6*$^{+/+}$ mice ($F_{2,30} = 3.286$, $P = 0.0435$; Fig. 2C), suggesting the involvement of glutamate in the regulation of memory by MCH neurons. Although there were no statistically significant differences when compared with *Pmch-Cre;Slc17a6*$^{flox/+}$, memory tended to be progressively better from the *Pmch-Cre;Slc17a6*$^{+/+}$ to *Pmch-Cre;Slc17a6*$^{flox/+}$ to *Pmch-Cre;Slc17a6*$^{flox/flox}$ mice. This trend suggests an association between the amount of glutamate released from MCH neurons and memory regulation.

Inducing acute vGlut2 cKO in MCH neurons enhanced broad object-related memory in mice

As shown above, when *Pmch-Cre* and *Slc17a6*$^{flox/flox}$ mice were crossed, mice with vGlut2 cKO in MCH neurons showed improved memory in the NOR test. However, vGlut2 cKO was performed at the prenatal stage, and the lack of vGlut2 in MCH neurons might trigger biological compensation during development. The present experiment was unable to exclude the possibility that the unknown compensatory activities affect the memory of affected mice rather than a lack of vGlut2 in MCH neurons.

To test the hypothesis that acute glutamatergic signaling loss from MCH neurons in mature mice exerts the same effect on memory, we performed vGlut2 cKO by in vivo genome editing using the CRISPR/Cas9 system (31, 32). To do this, we first generated an MCH neuron-specific Cas9-expressing mouse line by crossing *Pmch-Cre* mice with *Rosa26*$^{LSL\text{-}Cas9}$ mice (*Pmch-Cre;Rosa26*$^{LSL\text{-}Cas9}$; Fig. 3A). In these mice, Cas9 is coexpressed with the enhanced green flourescent protein (Cas9-EGFP) in the presence of Cre activity. IHC revealed that 98.1 ± 1.6% of MCH-immunoreactive (MCH-ir) neurons expressed Cas9-EGFP, and 98.2 ± 0.8% of Cas9-EGFP cells were MCH-ir neurons ($n = 3$; Fig. 3B). These observations demonstrated that the expression of Cas9 was restricted primarily to MCH neurons, ruling out any ectopic expression of Cas9 in other cells. Next, to induce a vGlut2 cKO by frameshift mutation, we designed two 20-bp sgRNAs targeting the *Slc17a6* gene, one of which cleaves exon 2 and the other of which cleaves exon 3 of this gene (Fig. 3C). A mixture of AAVs carrying two separate *Slc17a6* sgRNAs (*Slc17a6* sgRNA1 and 2) was used to increase the success rate of vGlut2 cKO. The LacZ protein, commonly used as a reporter in genetic engineering (33), is absent from the mouse genome, so we used sgRNA targeting *LacZ* as the control in this study. Stereotaxic injections of AAV-sgRNA-FLEX-mCherry of *Slc17a6*(sgRNAs) or *LacZ*(sgRNA) into the LHA of *Pmch-Cre;Rosa26*$^{LSL\text{-}Cas9}$ mice (Fig. 3D; hereafter referred to as MCH-vGlut2.cKO or MCH-LacZ mice, respectively) resulted in the expression of mCherry in Cas9-expressing neurons (82.0 ± 1.3% and 83.7 ± 1.3% for the MCH-LacZ and MCH-vGlut2.cKO mice, respectively; Fig. 3E and F). In addition,

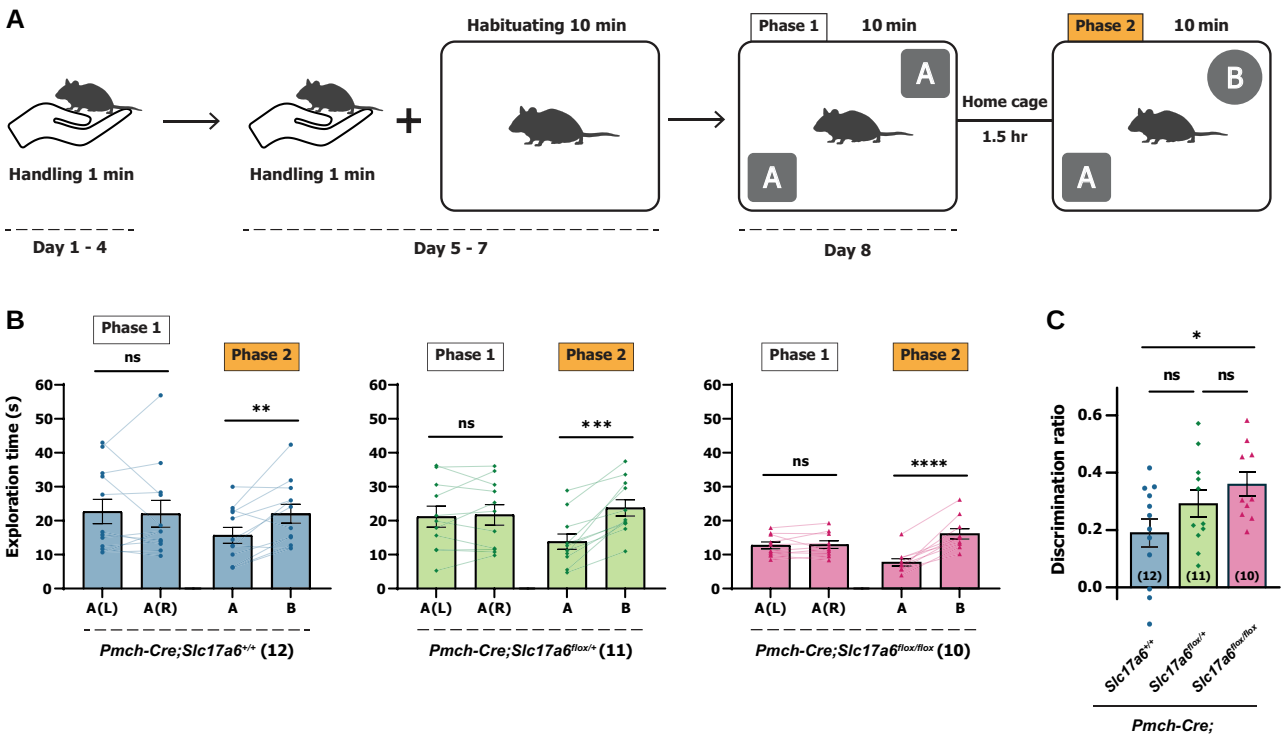

Fig. 2. Higher discrimination ratio in *Pmch-Cre;Slc17a6*$^{flox/flox}$ than in *Pmch-Cre;Slc17a6*$^{+/+}$ mice in the NOR test. A) Schematic illustration of the schedule and the procedure for the NOR test. B, C) Exploration time (in each phase) and discrimination ratio of the three mouse genotypes in the NOR test. A (L) and A (R): left and right identical objects in phase 1, respectively; A and B: familiar and novel objects in phase 2, respectively. The number of mice per group is shown in parentheses. The data are presented as dot plots; the bar graphs show means ± SEMs, and differences in the means were evaluated by paired *t* tests (B) or one-way ANOVA followed by a Tukey post hoc test (C); $^{*}P < 0.05$; $^{**}P < 0.01$; $^{***}P < 0.001$; $^{****}P < 0.0001$. ns, not significant.

90.2 ± 2.3% and 90.3 ± 1.5% of mCherry-expressing neurons were positive for Cas9-EGFP after the *LacZ*(sgRNA) and *vGlut2*(sgRNAs) injections, respectively (Fig. 3E and F'). Although sgRNA-expressing AAVs infected the cells in a nonspecific manner and induced sgRNA expression in infected cells, genome editing occurred only in the MCH neurons because a complex of Cas9 and sgRNA was required for this process. As reported above, Cas9 was specifically coexpressed in MCH neurons, so these results excluded any off-target effects in other neurons. According to the IHC results for MCH-vGlut2.cKO mice, none of the MCH-neuron axons in the CA1 were colocalized with the vGlut2 signal (0/51 axons from 3 mice; Fig. S1A, right column, and B). We observed that a large proportion of the MCH neuronal population was infected by AAVs, which was sufficient to assess the effects of the target genes.

Four weeks after injection, MCH-vGlut2.cKO and MCH-LacZ mice were subjected to a NOR test with a 1.5-h retention between the two phases (Fig 4A, upper panel). In this experiment, mice from both groups spent equal amounts of time exploring two identical objects in the encoding period (phase 1) and more time exploring the novel object than the familiar object in the retrieval period (phase 2; Fig. S2A). The discrimination ratio for MCH-vGlut2.cKO mice was significantly higher than that of MCH-LacZ mice ($t_{14} = 3.127$, $P = 0.0074$; Fig. 4B, left). Therefore, acute glutamatergic signaling loss in MCH neurons also improved memory, similar to prenatal vGlut2 cKO in MCH neurons, and sgRNA targeting *LacZ* did not affect memory function. These results indicated the role of glutamatergic signaling from MCH neurons in regulating short-term object recognition memory. To elucidate the extent of this effect further, we increased the retention interval to 48 h and 7 days (Fig. 4A, upper panel). In the 48-h retention trial, the ability to distinguish the novel object from the familiar object was still significantly higher in the MCH-vGlut2.cKO group than in the control group, as shown by the higher discrimination ratio ($t_{15} = 2.229$, $P = 0.0415$; Figs. 4B, middle, and S2B). The findings indicated that vGlut2 cKO in MCH neurons enhances both short- and long-term memory in the mouse model. Nevertheless, the long-term memory enhancement was not retained beyond 7 days ($t_{14} = 0.407$, $P = 0.6901$; Figs. 4B, right, and S2C).

We next examined whether location-related memory was also elevated in MCH-vGlut2.cKO mice using the object location (OL) test paradigm (34–36) (Fig 4A, lower panel). In this experiment, mice encountered two identical objects in an open arena where black adhesive tape was attached to one wall to serve as a spatial cue for the mice in navigating the environment. After 1.5 h of intertrial retention, one object was moved to another position, and the mice were allowed to re-explore the environment. In this experiment, MCH-vGlut2.cKO mice outperformed MCH-LacZ mice in discriminating the novel location of the object ($t_{15} = 2.145$, $P = 0.0487$; Fig. 4C) by spending more time exploring the displaced object than did MCH-LacZ mice (Fig. S2D). Together with the results of prenatal vGlut2 cKO in MCH neurons, these data firmly support the role of glutamatergic signaling from MCH neurons in general object-related memory regulation and both short- and long-term perspectives.

vGlut2 cKO in MCH neurons strengthened social recognition memory in mice

Social memory is critical for the survival and development of animals in their society, especially highly territorial species, such as rodents (37). We performed a three-chamber test to confirm the possibility of social memory enhancement in mice lacking

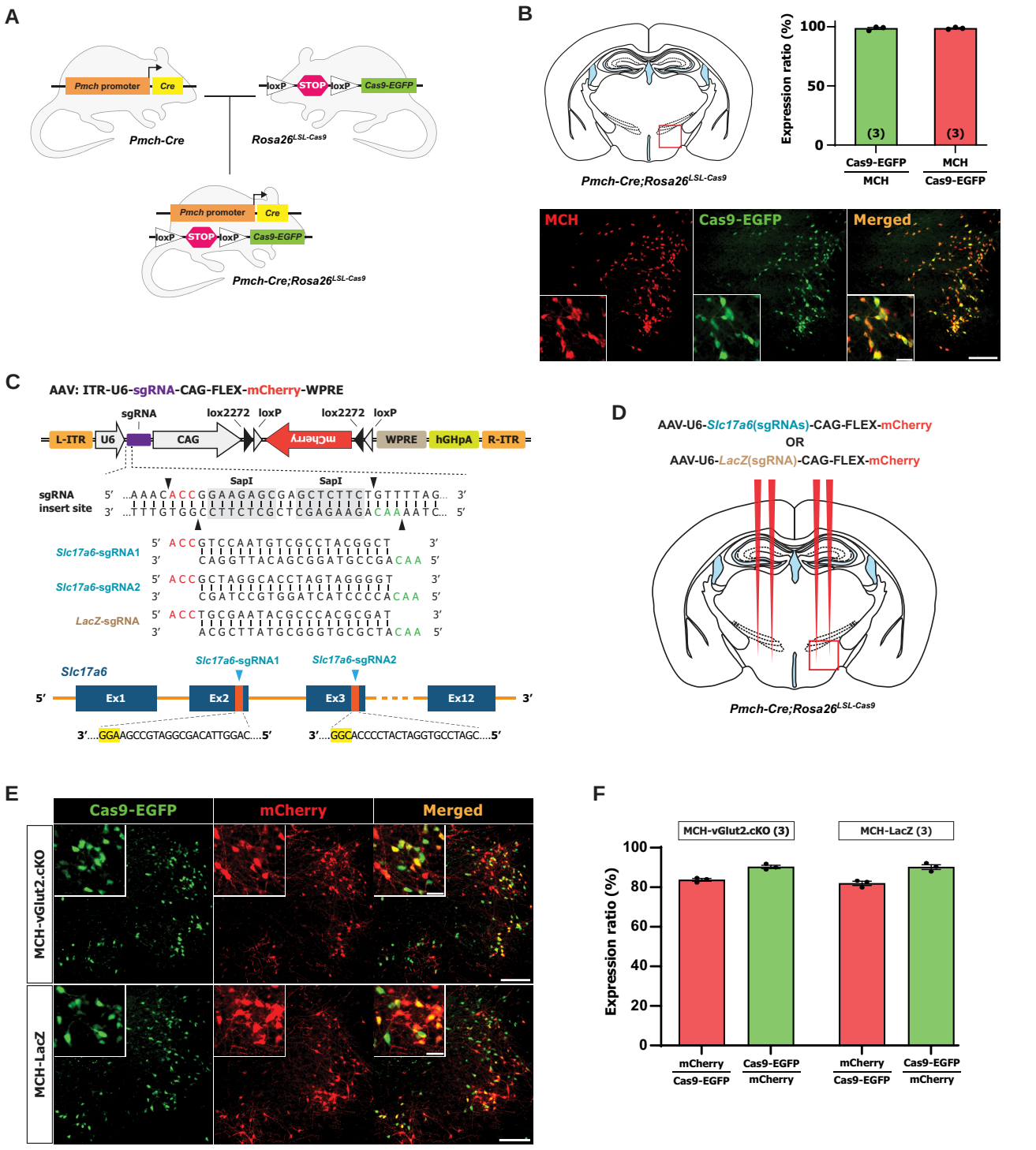

Fig. 3. The workflow for vGlut2 cKO in MCH neurons specifically using the CRISPR/Cas9 system. A) Generation of *Pmch-Cre;Rosa26*$^{LSL\text{-}Cas9}$ bigenic mice. B) Quantitative cell counts and representative immunohistochemical images showing the expression of Cas9 exclusively in MCH neurons. C) Construction of a plasmid carrying the sgRNA of interest by inserting the designed sgRNA into the plasmid backbone at the SapI restriction enzyme site (arrowheads). The image at the bottom shows the *Slc17a6* gene construct and cleavage sites for *Slc17a6* sgRNAs (arrowheads). D) AAV injection targets in the LHA. E, F) Representative immunohistochemical images and quantitative cell counts showing the expression of mCherry and Cas9-EGFP in MCH neurons after AAV injection. The data are presented as dot plots; the bar graphs show means ± SEMs. The scale bars: 200 μm in the large images and 50 μm in the small images. hGHpA, human growth hormone poly A signal.

glutamatergic signaling from MCH neurons (Fig. 5A). After the habituation session (phase 1), the mice were tested for their innate preference between a novel conspecific and an inanimate object (phase 2). The mice in both groups were more interested in exploring the stranger mouse (S1) than the object ($P = 0.0001$ and $P < 0.0001$ for MCH-LacZ and MCH-vGlut2.cKO, respectively; Fig. 5B). Moreover, there were no differences in the amount of time spent exploring S1 ($P = 0.1327$) or the object ($P = 0.9696$) between the two groups of mice (Fig. 5B). These results implied that the sociability of the mice, or their social motivation, in

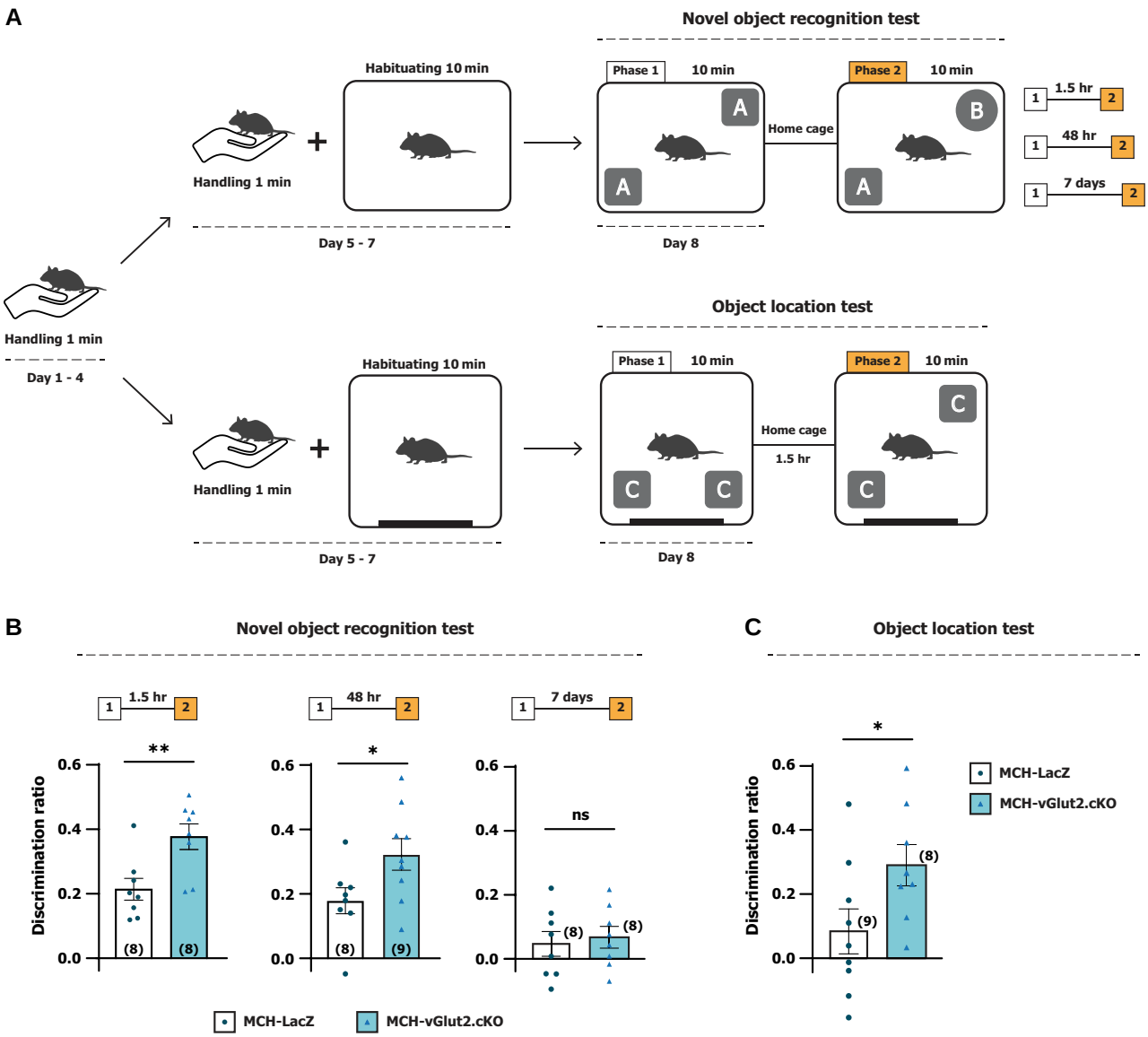

Fig. 4. Enhancement of the discrimination ratio in the NOR and OL tests after vGlut2 cKO in MCH neurons by CRISPR/Cas9. A) Schematic illustration of the schedule and procedure for the NOR test with different retention periods (upper panel) and the OL test (lower panel). B, C) Discrimination ratio in the NOR and OL tests, respectively, between the mouse groups. The number of mice per group is shown in parentheses. The data are presented as dot plots; the bar graphs show the means ± SEMs; and differences in the means were evaluated using unpaired *t* tests; $^{*}P < 0.05$; $^{**}P < 0.01$. ns, not significant.

both groups was unaffected (either impaired or enhanced). Subsequently, in phase 3, the object was replaced by another stranger mouse (S2), and the subject mice were tested for their social novelty and the ability to discriminate the novel conspecific from the familiar conspecific. Both groups spent more time interacting with S2 than S1 ($P = 0.0477$ and $P < 0.0001$ for MCH-LacZ and MCH-vGlut2.cKO, respectively; Fig. 5C), which indicated that the ability to recognize social novelty remained intact in both groups of mice. Interestingly, while there was no difference in S1 exploration between the two groups ($P = 0.8626$; Fig. 5C), the amount of time that MCH-vGlut2.cKO mice explored S2 was significantly greater than that of MCH-LacZ ($P = 0.0064$; Fig. 5C), which in turn led to a considerably greater ability to discriminate the novel conspecific ($t_{15} = 2.630$, $P = 0.0189$; Fig. 5D) by mice in the MCH-vGlut2.cKO group. All the evidence excluded two possible explanations for the higher discrimination ratio in MCH-vGlut2.cKO mice: (i) the impairment, specifically, of sociability and social novelty in MCH-LacZ mice or (ii) the increase in sociability of MCH-vGlut2.cKO mice. Because acquired social memory is the reference for animals to distinguish novel stimuli from familiar stimuli, a reasonable explanation for the greater ability of MCH-vGlut2.cKO alone to recognize social novelty is that it results from enhanced social recognition memory after vGlut2 cKO from MCH neurons.

vGlut2 cKO in MCH neurons had no significant effect on mouse body weight or energy expenditure

After MCH neuronal ablation, the mice showed metabolic abnormalities, such as reduced fat weight and increased energy consumption (18). Regarding the contribution of glutamatergic signaling from MCH neurons to these metabolic functions, previous reports have shown opposing results despite using the same mouse model (*Pmch-Cre*;*Slc17a6*$^{flox/flox}$ vs. *Slc17a6*$^{flox/flox}$) but different *Pmch-Cre* mouse strains (27, 29). To resolve this contrariety, we

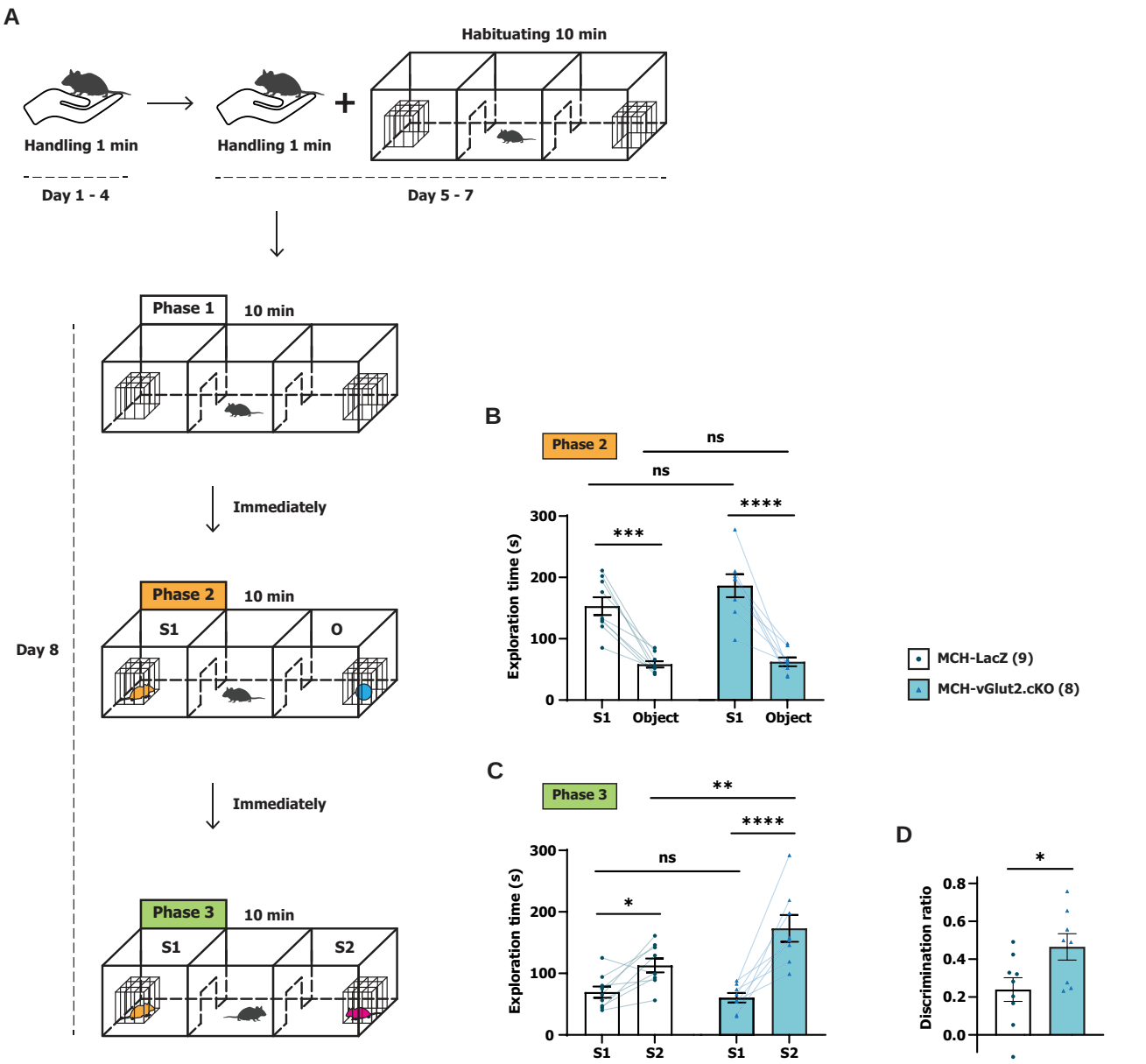

Fig. 5. Enhancement of the discrimination ratio in the three-chamber test after vGlut2 cKO in MCH neurons by CRISPR/Cas9. (A) Schematic illustration of the schedule and the procedure for the three-chamber test. S1, Stranger 1; S2, Stranger 2; and O, Object. B–D) Exploration time in each phase (B, C), and discrimination ratio between the mouse groups (D) in the three-chamber test. The number of mice per group is shown in parentheses. The data are presented as dot plots; the bar graphs show the means ± SEMs. Differences in the means were evaluated using two-way repeated-measures ANOVA with a Šidák post hoc test (B and C) or unpaired *t* tests (D); $^{*}P < 0.05$; $^{**}P < 0.01$, $^{***}P < 0.001$; $^{****}P < 0.0001$. ns, not significant.

used alternative mouse models (*Pmch-Cre;Slc17a6*$^{+/+}$ vs. *Pmch-Cre;Slc17a6*$^{flox/+}$ vs. *Pmch-Cre;Slc17a6*$^{flox/flox}$) to measure the metabolic rate. The body weight and total food intake of the mice were measured weekly from the age of 4 to 15 weeks. In general, there was no significant difference in body weight or weekly caloric intake across all mouse genotypes at almost any time point, except for the lower weight of *Pmch-Cre;Slc17a6*$^{flox/flox}$ mice compared with *Pmch-Cre;Slc17a6*$^{+/+}$ mice at 4 and 5 weeks of age ($P = 0.0147$ and $P = 0.0054$, respectively) (Fig. 6A and B). At 16 weeks of age, the three genotypes also showed no significant differences in oxygen consumption, respiratory quotient, or locomotor activity in 24 h or during the individual light and dark periods (Fig. 6C–H). These results suggested that glutamate from MCH neurons had little or no apparent effect on body weight or energy expenditure.

Discussion

MCH neurons play essential roles in regulating various functions by extensively projecting to different brain regions via several neurotransmitters, including the neuropeptides MCH, nesfatin-1, CART, and VEGF-A, or the classic neurotransmitter glutamate. The understanding of neurotransmitter signaling pathways other than MCH has remained vague, making it insufficient for understanding the role of MCH neurons. In this study, using cKO of *Slc17a6* gene mice, we investigated the role of glutamate from MCH neurons in regulating memory and metabolic rate. Interestingly, glutamatergic signaling loss from MCH neurons enhanced general memories in mice, including novel object, location, and social recognition memories but did not affect their energy metabolism.

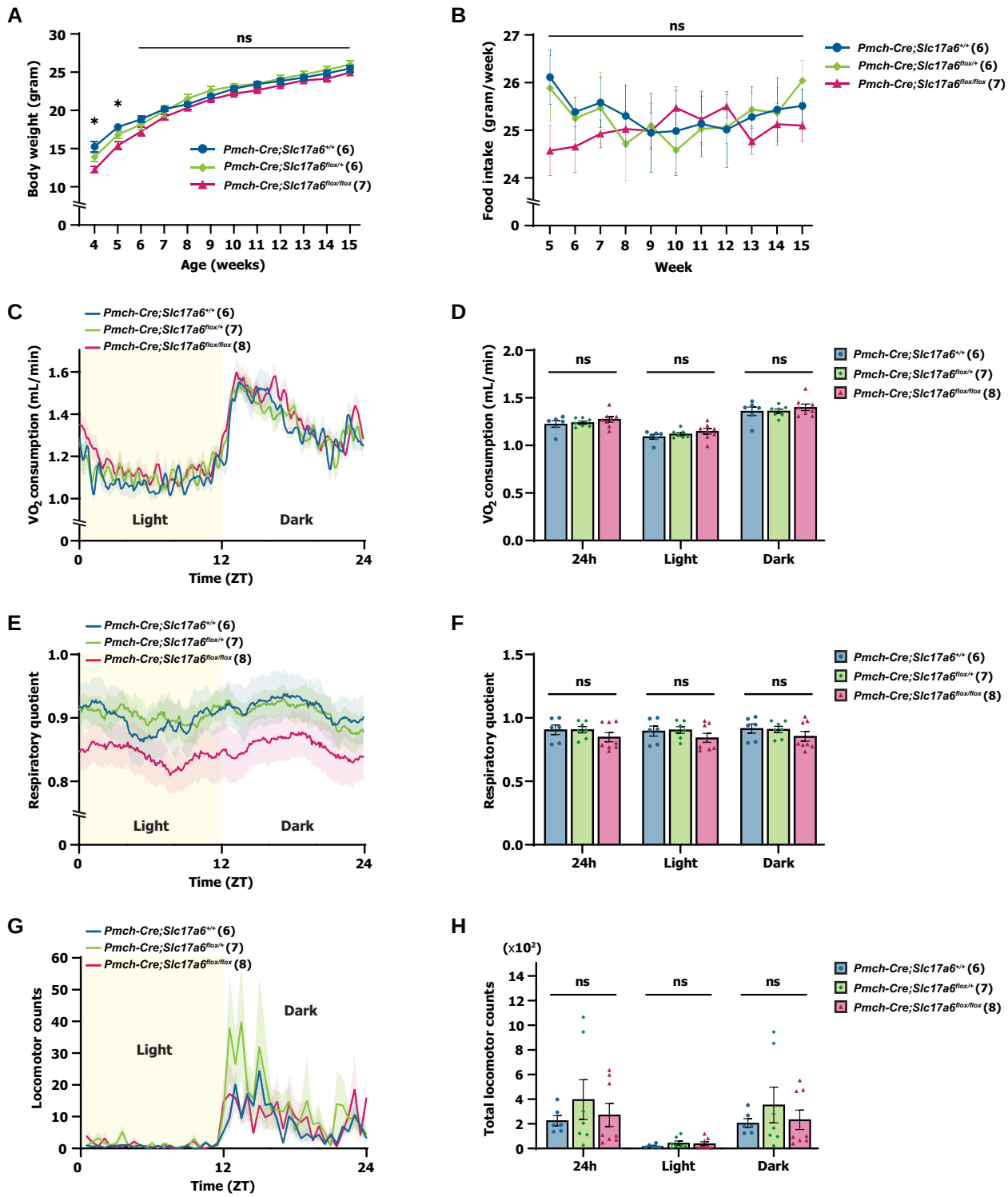

Fig. 6. No significant effect of vGlut2 cKO in MCH neurons on body weight, food intake, oxygen consumption, RQ, or locomotor activity. A, B) Comparison of body weight and food intake between three groups of mice aged from 4 to 15 weeks. Energy expenditure was measured as average daily oxygen consumption (C, D), RQ (E, F), and locomotor activity (G, H) at 16 weeks of age among the three mouse genotypes. The number of mice per group is shown in parentheses. The data are presented as dot plots; the bar graphs show means ± SEMs. Differences in means among the groups were determined by a two-way repeated-measures ANOVA with a Šidák post hoc test (A, B) or a one-way ANOVA (D, F, H); *$P < 0.05$. ns, not significant. Time is referenced to ZT.

MCH neurons are found primarily in the LHA and innervate various brain regions, such as the nucleus accumbens, ventral tegmental area, cortex, amygdala, hippocampus, thalamus, hypothalamus, and brainstem (9). From directly infusing MCH into the brain (11, 12) or MCHR1 KO (16), MCH is considered necessary to preserve memory through various mechanisms, including decreasing hippocampal long-term potential thresholds (38). Nevertheless, we previously reported that MCH neuronal ablation or inhibition of these neurons by manipulation techniques (optogenetics and chemogenetics) improves memory (10). These

results raised our concern about other spontaneous mechanisms by which MCH neurons prevent memory formation. These neurons release not only MCH but also glutamate and act as glutamatergic neurons. vGlut proteins (vGlut1, vGlut2, and vGlut3) package glutamate into vesicles at presynaptic areas. However, the majority of MCH neurons express vGlut2 exclusively, while a tiny proportion express vGlut3 but not vGlut1 (25). We hypothesized that vGlut2 cKO would entirely abolish glutamatergic signaling from these neurons. Utilizing Cre-loxP-dependent KO to disable vGlut2 in MCH neurons is a conventional approach that has been successfully demonstrated in previous studies (27, 29, 30). Using this approach, mice with vGlut2 cKO in MCH neurons exhibited improved short-term memory in the NOR test. However, by crossing *Pmch-Cre* mice with *Slc17a6*$^{flox/flox}$ mice, glutamatergic signaling was inhibited prenatally. We were unable to confirm whether there was any biological compensation for the lack of this signaling pathway during the development, which could have caused the memory improvement rather than a lack of vGlut2 itself. To address this concern, we used the CRISPR/Cas9 system to knockout *Slc17a6* in MCH neurons in mature mice. Interestingly, this method demonstrated the same phenomenon: inhibiting glutamate released from MCH neurons also increased short-term memory in the NOR test. Moreover, the long-term novel object memory and location-related memory were also strengthened. This enhancement was not restricted to object-related memory alone but was also observed in social recognition memory, as shown in the three-chamber test. These results suggest that (i) in addition to MCH, MCH neurons also use glutamate to regulate memory, and (ii) other modulators cannot compensate for the loss of glutamatergic signaling. MCH neurons are critical for regulating sleep and wakefulness, especially for promoting and sustaining REM sleep (39). In addition, the MCH neuronal subpopulation activated during REM sleep is involved in forgetting hippocampal memories (10). Inhibiting glutamatergic signaling from MCH neurons decreases REM sleep for a short time in the dark period without affecting sleep structure, non-REM sleep, or wakefulness. MCH neurons lacking glutamate can still promote REM sleep (30). These findings suggest that, in our study, the general memory improvement in mice with selective vGlut2 cKO in MCH neurons was not due to the non-REM or REM sleep time alterations.

Several investigators have reported contrary findings regarding the effect of MCH neuronal glutamate on energy homeostasis. Schneeberger et al. (27) reported that compared with *Slc17a6*$^{flox/flox}$ mice, *Pmch-Cre;Slc17a6*$^{flox/flox}$ mice [using the Tg(*Pmch-cre*)^{1Rck}/J19 strain] had a lower body weight, hyperactivity, late-onset hypophagia, lower leptin level, improved glucose tolerance, and loss of sucrose preference. Meanwhile, another study, using the same mouse model comparison *Slc17a6*$^{flox/flox}$ vs. *Pmch-Cre;Slc17a6*$^{flox/flox}$ but a different *Pmch-Cre* mouse strain [Tg(*Pmch-cre*)^{1Lowl}/J], found no effect of vGlut2 cKO in MCH neurons on body weight, blood glucose levels, feeding, oxygen consumption, locomotor activity, or body temperature (29). In the two studies mentioned above, using *Slc17a6*$^{flox/flox}$ mice as a control group to compare with *Pmch-Cre;Slc17a6*$^{flox/flox}$ mice may have some limitations due to the potential effect on the metabolism of Cre expression or *Pmch-cre* gene insertion into anonymous chromosomes. To resolve this, we compared *Pmch-Cre;Slc17a6*$^{+/+}$, *Pmch-Cre;Slc17a6*$^{flox/+}$, and *Pmch-Cre;Slc17a6*$^{flox/flox}$ mice using *Pmch-Cre* mice with [Tg(*Pmch-cre*)^{1Lowl}/J] background. The body weight of *Pmch-Cre;Slc17a6*$^{flox/flox}$ mice was lower than that of *Pmch-Cre;Slc17a6*$^{+/+}$ mice only when the mice were 4 and 5 weeks of age. This lower body weight could be explained by the fact that mouse pups were mainly nurtured by maternal milk before they were 4 weeks old (weaning time point). During this period, the size of pups, or physical development in general, is significantly affected by feeding conditions such as parental mental and physical health, care, or the quantity of pup littermates (40). After weaning and isolation, *Pmch-Cre;Slc17a6*$^{flox/flox}$ mice started to reach the average weight of the two other groups from 6 weeks of age and maintained this condition until they were at least 15 weeks old, as demonstrated in the present study. Our findings support no significant effect of glutamate in MCH neurons on body weight in general, caloric intake, or energy expenditure. Therefore, our results are consistent with those of Sankhe et al. (29), but not with those of Schneeberger et al. (27). These inconsistent results may stem from the use of different *Pmch-Cre* mouse strains between the studies, as discussed previously (29). The authors were concerned with the ectopic expression of Cre outside MCH neurons in the Tg(*Pmch-cre*)^{1Rck}/J19 mouse strain and the subsequent off-target effect of vGlut2 cKO on metabolism. Moreover, MCH neuronal ablation, MCH KO, and MCHR1 KO have been consistently reported to increase energy expenditure and reduce fat weight (2, 18, 41, 42), and an MCHR1 antagonist caused hypophagia in an MCHR1-KO model (43). It seems that MCH, rather than glutamate, might play an important role in the metabolic regulation of MCH neurons.

Our findings confirmed that glutamate is an essential neurotransmitter used by MCH neurons to regulate memory but not to control metabolism. Using the three-chamber test has some limitations in assessing social memory because the complexity of this memory type cannot be entirely expressed through sociability and social novelty ability after short-term familiarization (44). Other facets, such as kin relationships, social ranks, and mates, are also parts of social memory and require much more comprehensive behavioral models to assess. In addition to these limitations, questions remain to be addressed. For example, is this glutamatergic signaling also involved in other types of memory in addition to novel object-related, spatial, and social recognition memories? NOR, OL, and three-chamber tests are non- or minimal-stress memory tests. We believe that this signaling pathway also contributes to emotion- or stress-facilitated memory, such as contextual fear or cued fear memories, at least to some extent. Or, which neural circuits or pathways for memory regulation are primarily affected by glutamate released from MCH neurons? Despite the involvement of various brain areas, object-related, spatial, and social memories are considered hippocampus dependent (45, 46). Activating MCH neurons increases the frequency and amplitude of inhibitory postsynaptic potentials in pyramidal neurons in the hippocampus. MCH neurons seem to be pivotal for hippocampus-dependent memory (10). Our findings suggest that direct glutamatergic signaling from MCH neurons in the hypothalamus to the hippocampus is mainly responsible for memory regulation. Other pathways must also be considered, such as the dense projection from MCH neurons to the lateral septum, which is an area with multifaceted functions in controlling reward, memory, feeding, and emotion (26, 47). Another issue is that although a lack of glutamate from MCH neurons enhances memory, we cannot confirm the natural function of this signaling pathway in memory. Does it prevent encoding information, or inhibit memory consolidation, or delay retrieval? The microcircuits between MCH neuronal terminals and target neurons warrant further investigation to address this concern. Finally, whether other neurotransmitters released from MCH neurons contribute to the regulation of memory and metabolism also warrants investigation. There is little evidence of a role for CART, nesfatin-1, or VEGF-A in these functions of MCH neurons. Understanding the roles of these neurotransmitters may elucidate the unknown functions of MHC neurons and reveal their potential roles in related neuropsychiatric or metabolic disorders.

Materials and methods

Ethical approval

The Institutional Animal Care and Use Committee of the Research Institute of Environmental Medicine, Nagoya University, and CIBR approved all the experimental procedures involving animals (approval numbers R210096 and R210729 for Nagoya University and CIBR-IACUC-058 for CIBR). All efforts were made to minimize animal use and any discomfort or pain.

Animals

Mice were housed in dedicated animal facility cages, allowed access to food and water ad libitum, and maintained in a controlled environment at an average temperature of 22–23.5 °C under a 12/12-h light/dark cycle (light on at zeitgeber time [ZT] 0 [light] and light off at ZT 12 [dark]). All experiments were conducted using male mice.

The mouse lines used were *Pmch-Cre* (Tg(*Pmch-cre*)^{1Lowl}/J, #014099; Jackson Laboratory, Bar Harbor, ME, USA), *Slc17a6*^{flox} (*Slc17a6*^{tm1Lowl}/J, #012898; Jackson Laboratory), which possess loxP sites flanking exon 2 of *Slc17a6*, Ai14 (*Rosa26*$^{LSL\text{-}tdTomato}$; B6.Cg-*Gt(ROSA)26Sor*$^{tm14(CAG\text{-}tdTomato)Hze}$/J, #007914; Jackson Laboratory) and *Rosa26*$^{LSL\text{-}Cas9}$ (B6J.129(B6N)-*Gt(ROSA)26Sor*$^{tm1(CAG\text{-}cas9*,\text{-}EGFP)Fezh}$/J, #026175; Jackson Laboratory), which possess a STOP-flox cassette preventing expression of the downstream bicistronic sequences (*Cas9* and *EGFP*). All strains were maintained on a C57BL/6J genetic background. Wild-type C57BL/6J mice were obtained from CLEA Japan (Tokyo, Japan).

To generate three genotypes of *Slc17a6*^{flox} (wild type, heterozygous, and homozygous) in *Pmch-Cre* mice, we initially crossed *Pmch-Cre*$^{Tg/Tg}$ mice with *Slc17a6*$^{flox/flox}$ mice. The F1 offspring (*Pmch-Cre*$^{Tg/0}$;*Slc17a6*$^{flox/+}$) were crossed back with *Pmch-Cre*$^{Tg/Tg}$ mice, and only the F2 offspring (*Pmch-Cre*$^{Tg/Tg}$; *Slc17a6*$^{flox/+}$) were used for self-mating to generate the following three bigenic strains: *Pmch-Cre*$^{Tg/Tg}$;*Slc17a6*$^{+/+}$, *Pmch-Cre*$^{Tg/Tg}$;*Slc17a6*$^{flox/+}$, and *Pmch-Cre*$^{Tg/Tg}$; *Slc17a6*$^{flox/flox}$ (hereafter referred to as *Pmch-Cre;Slc17a6*$^{+/+}$, *Pmch-Cre; Slc17a6*$^{flox/+}$, and *Pmch-Cre;Slc17a6*$^{flox/flox}$, respectively). The *Pmch-Cre; Rosa26*$^{LSL\text{-}tdTomato}$;*Slc17a6*$^{+/+}$ and *Pmch-Cre;Rosa26*$^{LSL\text{-}Cas9}$ mouse lines were generated by mating *Pmch-Cre*$^{Tg/Tg}$ mice with *Rosa26*$^{LSL\text{-}tdTomato}$ and *Rosa26*$^{LSL\text{-}Cas9}$ mice, respectively.

Genotyping and DNA sequencing

Mouse brain tissues were fixed in 10% formalin (066-03847; Fujifilm Wako Pure Chemical Industries, Osaka, Japan), and DNA was extracted using the REDExtract-N-Amp Tissue PCR Kit (XNAT; Sigma-Aldrich, St Louis, MO, USA), according to the manufacturer's instructions with minor modifications. In brief, for each sample (2 mm mousetail tip or 4 to 5 brain slices from a specific area), we prepared a premixed solution of 24 µL extraction solution and 6 µL tissue preparation solution (4:1 ratio). The sample was added to the mixture, vortexed, and incubated at room temperature for 10 min and then at 95 °C for 3 min. Then, 25 µL neutralization solution was added, and the sample was stored at 4 °C for up to 6 months until use.

After extraction, crude genomic DNA was amplified using the KOD FX Neo procedure (KFX-201; Toyobo, Kita, Osaka, Japan). We prepared 10 µL reactions containing Milli-Q water (1.6 µL), 2×PCR buffer for KOD FX Neo (5 µL), 2 mM dNTPs (2 µL), 10 pmol/µL primers #1 (0.1 µL) and #2 (0.1 µL), template DNA (1 µL), and 1.0 U/µL KOD FX Neo (0.2 µL). Based on the *Slc17a6* sequence (accession no. NC_000073.7) and the original procedure for generating the *Slc17a6*^{flox} mouse line (48), the following primer pairs were used (Primer3, web version 4.1.0; https://primer3.ut.ee/): primer pair 1 (5′-CCTGAGCGAAGGTGAGCTGAA-3′ and 5′-CCAAATACCTGAAAGTTACTG-3′), the outer primer pair (5′-TGGTGTTAAAATTCCATAGGC-3′ and 5′-GGTGCACAGTTGAAGGTTC-3′), and the inner primer pair (5′-TGGTGTTAAAATTCCATAGGC-3′ and 5′-GCTGTATAAAATGTCAAGGCC-3′). The positions of each primer pair are illustrated in Fig. 1B and C. Primer pair 1 was used to identify the *Slc17a6*^{flox} genotype using mousetail samples via the following PCR step-down cycle method: 94 °C for 3 min → (94 °C for 20 s → 64 °C for 1 min → 72 °C for 1.5 min) for 3 cycles → (94 °C for 20 s → 60 °C for 1 min → 72 °C for 1.5 min) for 5 cycles → (94 °C for 20 s → 56 °C for 1 min → 72 °C for 1.5 min) for 27 cycles → 72 °C for 10 min → 4 °C. The *Slc17a6*^{flox} genotype of the mice was determined for the behavioral experiments. Outer and inner primer pairs were used for nested PCR to confirm vGlut2 cKO in MCH neurons in the LHA, hippocampus, and cortex excised from brain slices of mice from the three genotypes: *Pmch-Cre;Slc17a6*$^{+/+}$, *Pmch-Cre;Slc17a6*$^{flox/+}$, and *Pmch-Cre;Slc17a6*$^{flox/flox}$. For each round of PCR, we used the following PCR three-step cycle method: 94 °C for 3 min → (94 °C for 20 s → 60 °C for 30 s → 72 °C for 3 min) for 35 cycles → 72°C for 10 min → 4 °C. The PCR product from the first PCR round was used as the DNA template in the second round.

The PCR products were purified from agarose gels using the FavorPrep GEL/PCR purification kit (FAGCK 001; Favorgen Biotech, Ping Tung, Taiwan). Then, these products were subcloned using the Zero Blunt TOPO PCR Cloning Kit (450245; Invitrogen, Waltham, MA, USA). The linearized and topoisomerase I-activated pCR Blunt II-TOPO vector and salt solution were mixed with the PCR products, and incubated at room temperature for 10 min and then transformed into *Escherichia coli* DH5α competent cells following a standard heat shock protocol (in which the cells were thawed on ice, 3 µL of ligation mix was added, the tube was flicked four or five times, the tube containing the cells and ligation mix was placed on ice for 30 min, the cells were then heat shocked by incubating the tube containing them at 42 °C for 45 s, placing it on ice for 5 min, adding 200 µL of Plus Grow II medium, and then incubated it at 37 °C for 1 h). After the transformation, the cells were plated on LB agar supplemented with kanamycin and incubated at 37 °C for ∼16 h. Well-isolated, healthy colonies were picked up and grown in 2 mL of Plus Grow II medium supplemented with 0.1% kanamycin at 37 °C for 1 day. The plasmids were purified using the Cica Geneus Plasmid Prep Kit (08207-96; Kanto Chemical Co., Portland, OR, USA) and confirmed by EcoRI-HF restriction digestion (R3101; New England Biolabs, Ipswich, MA, USA). Finally, the correct plasmids were sequenced using the M13 forward (5′-GTAAAACGACGGCCAG-3′) and reverse (5′-CAGGAAACAGCTATGAC-3′) primers.

Plasmid construction

Using the CRISPR/Cas9 system (31) to knockout gene(s) of interest with high specificity and minimal off-target effects, we designed single-guide RNAs (sgRNAs) based on CHOPCHOP (https://chopchop.cbu.uib.no/). To knockout *Slc17a6* gene, two sgRNA candidates were selected to target the following sequences: 5′-CAGGTTACAGCGGATGCCGAAGG-3′ (in exon 2) and 5′-CGATCCGTGGATCATCCCCACGG-3′ (in exon 3). A sgRNA targeting the *LacZ* gene (target sequence: 5′-TGCGAATACGCCCACGCGATGGG-3′) was used as the control. This gene is not in the mouse genome and has been widely used in previous studies (49, 50). U6-sgRNA(backbone)-CAG-FLEX-mCherry-WPRE was used as the vector plasmid for sgRNA insertion at the SapI site in the

sgRNA(backbone) area. This plasmid vector was created by inserting the U6-sgRNA(SapI) fragment of pAAV-U6-sgRNA(SapI)-hSyn-GFP-KASH-bGH (Addgene #60958) into pAAV-CAG-FLEX-mCherry-WPRE (produced in house). DNA sequencing using the U6 promoter as the template and the forward primer 5′-CTGAGGGCC TATTTCCCATG-3′ confirmed the correct insertion of the sgRNA.

Production and purification of AAV vectors

The AAV Helper-free system (Agilent Technologies, Santa Clara, CA, USA) was used to produce all AAV vectors in this study based on the calcium phosphate transfection method. Before transfection, several plates of healthy cultured HEK-293 cells in Dulbecco's modified Eagle's medium-high glucose (DMEM; Sigma-Aldrich Merck, Darmstadt, Germany) at 90–95% confluence were prepared. On the day of transfection, a solution of 0.3 M $CaCl_2$ (1 mL/plate), pAAV containing the gene of interest (10 µg/plate), pAAV-Capsid (serotype 9; 10 µg/plate), and pHelper (10 µg/plate) was slowly added to 2× HEPES buffer saline (1 mL/plate) slowly dropwise under continuous vortexing. The mixture was then allowed to stand for ∼15 min at room temperature and added dropwise to the plates (2 mL/plate). The DMEM in the plates was changed within 24 h. Three days after transfection, the transfected cells and medium were collected and centrifuged. After discarding the supernatant, the pellet was rinsed with phosphate-buffered saline (PBS), centrifuged, and resuspended in Hank's balanced salt solution. The cell suspension was then subjected to three or four freeze–thaw cycles to disrupt the cells; each cycle consisted of freezing at −80 °C for ≥30 min, thawing in a water bath at 37 °C for 3 min, and vortexing at room temperature for 1 min. Subsequently, the cell suspension was centrifuged at 4 °C for 10 min. After transferring the supernatant to a new tube, 1 µL of benzonase nuclease was added (0.025 U; Merck, Darmstadt, Germany), and the mixture was incubated in a water bath at 37 °C for 30 min. The solution was centrifuged at 14,000 rpm at 4 °C for 10 min several times until the supernatant was sufficiently transparent to be divided into aliquots. Finally, quantitative PCR was performed to titrate the purified AAV. AAV aliquots were stored at −80 °C until use.

Stereotaxic injection of virus

Surgeries and injections of AAV were performed on 9- to 10-week-old *Pmch-Cre;Rosa26*$^{LSL\text{-}Cas9}$ mice using a stereotaxic instrument (David Kopf Instruments, Tujunga, CA, USA) under isoflurane (Fujifilm Wako Pure Chemical Industries) anesthesia (2% for the first 30 min and 1% after that). After ensuring that the mouse head was fixed firmly by a mouth holder and two ear bars, the scalp was incised, and the skull was drilled. The coordinates for the LHA injections in both hemispheres were AP (from Bregma), −1.5 mm; ML (from midline), ± 0.5 mm; DV (from brain surface), −5.2 mm; AP, −1.5 mm; ML, ± 0.9 mm; and DV, −5.0 mm. Viruses were injected through a pulled glass micropipette with a 50-µm-diameter tip (G150-4; Harvard Apparatus, Holliston, MA, USA) using an air pressure injector (Pneumatic PicoPump; World Precision Instruments, Sarasota, FL, USA) as follows: a mixture of AAV-U6-*Slc17a6*(sgRNA1)-CAG-FLEX-mCherry (5.5×10^{12} copies/mL) and AAV-U6- *Slc17a6*(sgRNA2)-CAG-FLEX-mCherry (5.5×10^{12} copies/mL) 1:1 by volume (600 nL/injection), AAV-U6-*LacZ*(sgRNA)-CAG-FLEX-mCherry (600 nL/injection, 4.7×10^{12} copies/mL) and AAV-CAG-FLEX-EGFP (600 nL/injection, 2.2×10^{13} copies/mL). Each injection was performed at an average rate of ∼100 nL/min, and the capillary was left in place for ∼10 min before it was retracted slowly to avoid viral leakage.

Immunohistochemistry

For results shown in Fig. 3, the mice were euthanized under deep anesthesia using isoflurane, followed by transcardial perfusion with 25 mL of chilled saline and 25 mL of chilled 10% formalin. Their brains were quickly removed, postfixed by immersion in 10% formalin solution overnight at 4 °C, and then for subsequent cryoprotection, they were immersed in 30% sucrose in PBS at 4 °C for at least 2 days or until they had sunk. After freezing in optimal cutting temperature compound (OTC 4583; Sakura Finetek, Osaka, Japan) at −80 °C, the brains were sliced coronally using a cryostat (CM3050-S; Leica Microsystems, Wetzlar, Germany) at 40 µm thickness and stored in PBS containing 0.05% NaN_3 at 4 °C until further staining. For staining, brain slices were washed with buffered protein and detergent to block nonspecific binding (1% bovine serum albumin and 0.25% Triton-X in PBS) three times and incubated with primary antibodies under gentle shaking at 4 °C overnight. The sections were rewashed with blocking buffer (three times) before being incubating with the corresponding secondary antibodies at room temperature for 1 h. The brain slices were mounted on glass slides (PRO-02; Matsunami Glass, Kishiwada, Osaka, Japan), coverslipped (C024401; Matsunami Glass), and sealed with nail polish before being examined under a fluorescence microscope (BZ-X710; Keyence, Osaka, Japan). The following primary antibodies diluted in blocking buffer were used: anti-MCH rabbit antibody (M8440; Sigma-Aldrich, St Louis, MO, USA) at 1:1,000, anti-GFP mouse antibody (mFX75; Fujifilm Wako Pure Chemical Corporation, Osaka, Japan) at 1:1,000, and anti-DsRed rabbit antibody (632496; Takara Bio, Shiga, Japan) at 1:1,000. The following secondary antibodies were used: CF 488-conjugated donkey antimouse antibody (20014; Biotium, Hayward, CA, USA) at 1:1,000 and CF 594-conjugated donkey anti-rabbit antibody (20152; Biotium) at 1:1,000. For cell counting, a series containing every fourth brain section of the LHA was examined under a fluorescence microscope (BZ-X710; Keyence). Brain regions were identified using the mouse brain atlas in stereotaxic coordinates by Paxinos and Franklin (second edition) (51).

For results shown in Fig. S1, the mice were deeply anesthetized and perfused with a 4% paraformaldehyde phosphate buffer solution (09154-85; Nacalai Tesque, Nakagyo, Kyoto, Japan). The brains were removed from the skull and postfixed in the same fixative overnight at 4 °C. Subsequently, the brains were cryoprotected in 20% sucrose overnight and frozen. The frozen brains were cut on a cryostat at 40 µm thickness. The floating sections were incubated with primary antibodies overnight at room temperature. The following antibodies were used: anti-GFP goat polyclonal (600-101-215; Rockland Immunochemicals, Pottstown, PA, USA) at 1:250, anti-vGlut2 rabbit polyclonal (MSFR106310; Frontier Institute, Hokkaido, Japan) at 1:1,000, anti-vGlut2 guinea pig polyclonal (MSFR106290; Frontier Institute) at 1:1,000, and anti-DsRed rabbit polyclonal (MSFR101400; Frontier Institute) at 1:1,000. The sections were then treated with species-specific secondary antibodies conjugated to Alexa Fluor 488 (A32814, A21206, Invitrogen; 706-545-148, Jackson ImmunoResearch Laboratories, West Grove, PA, USA), 555 (A31572, Invitrogen), or 647 (706-605-148; Jackson ImmunoResearch Laboratories) for 2 h at room temperature. Mounting medium (P36980, ProLong Glass Antifade Mountain, Thermo Fisher Scientific, Waltham, MA, USA) was applied to the sections, which were then mounted with coverslips (C024401; Matsunami Glass). Structured illumination microscopy (SIM)–super-resolution microscopy (SRM) microimages were obtained using a Zeiss ELYRA 3D-SIM system equipped with an EM-CCD camera (Carl Zeiss). Before acquiring

the SIM–SRM images, precise alignment for the different wavelengths of light was performed using the same mounting medium (ProLong Glass) containing 0.1% Tetraspeck (T7280, 0.2-μm beads; Thermo Fisher Scientific) to correct for unavoidable laser misalignment and optical aberrations, which can lead to the alignment not coinciding at very high resolution. Next, Z-section images were obtained at intervals of 126 nm using a 64× objective lens. The number of pattern rotations of the structured illumination was adjusted to 3 in the ELYRA system. After obtaining all the images, the SIM images were reconstructed and aligned using the channel alignment data. SRM images were analyzed using ImageJ (United States National Institutes of Health, http://rsb.info.nih.gov/ij/). The optimal brightness and grayscale pixel values were manually adjusted to provide the sharpest discrimination of the microstructure border. Images were obtained at three unselected locations within the hippocampal CA1 region. The percentage of vGlut2-positive MCH-neuron axons was estimated.

Memory tests

General procedure

For all memory tests, 10- to 12-week-old (*Pmch-Cre;Slc17a6*$^{+/+}$, *Pmch-Cre;Slc17a6*$^{flox/+}$, and *Pmch-Cre;Slc17a6*$^{flox/flox}$) mice or 13- to 26-week-old AAV-injected *Pmch-Cre;Rosa26*$^{LSL\text{-}Cas9}$ mice were subjected to the tests. Two weeks before starting the NOR and OL tests, the mice were separated into single cages. After completing the NOR and OL tests, mice were group-housed again for 5 weeks before starting the three-chamber test. For acclimation, the subject mice were gently handled for 7 days (1 min/day) and habituated to the specific arenas for 3 days (10 min/day) before each memory test. On the habituation and test days, the mice were transferred to the experiment room at least 1 h beforehand. The temperature of the experimental environment was 20.1–22.9 °C, the humidity was 20–26%, and the behavioral study area was illuminated by indirect diffusion light with an intensity of 12–13 lux measured on the surface of the arena floor. All materials used during the tests were cleaned thoroughly with 70% ethanol before and after each trial to prevent olfactory trails. Mouse behaviors were recorded by a video camera fixed above the arenas. All habituation sessions and tests were performed during ZT 15–24.

NOR test

The procedure was adapted from a method previously described elsewhere (10, 52). In phase 1 (encoding period), two identical objects (object A) were placed symmetrically in a blue acrylic arena (width × depth × height, 42 cm × 32 cm × 20 cm; Fig. S3A), and the mice were allowed to explore freely for 10 min. After an intertrial interval (1.5 h, 48 h, or 7 days) in their home cage, in phase 2 (retrieval period), the mice were returned to the arena to reexplore the objects for 10 min. In this phase, one of the two identical objects was replaced by a different object (object B) at the same position. Exploration was defined as sniffing objects or touching with the head toward objects, excepting behaviors such as biting, standing on the objects, or standing close to the objects without direct interaction. The time spent exploring each object was counted manually, and the discrimination ratio was calculated as $(time^{B} - time^{A})/(time^{A} + time^{B})$, where $time^{A}$ and $time^{B}$ refer to the time the mice spent exploring objects A and B, respectively, in phase 2. Object A was distinguishable from object B in shape, color, and material but nearly equal in size. Object pairs were chosen differently across tests to prevent acquired memory. All the objects were secured to the arena floor by double-sided adhesive tape. In the 48-h or 7-day retention trials, the mice were again habituated to the empty arena 1 day or 2 days before the test day of phase 2, respectively.

OL test

The procedure was adapted following a protocol described elsewhere (34). Mice were habituated and tested in a white acrylic arena (width × depth × height, 30 cm × 30 cm × 30 cm; Fig. S3B) with black tape stuck to a wall, which served as a spatial cue. In phase 1 (encoding period), two identical objects (object C) were placed at two corners close to the marked wall of the arena, 6 cm away from the close edges, and the mice were allowed to explore the whole arena freely for 10 min. After an intertrial interval of 1.5 h, in phase 2 (retrieval period), one object was relocated to the opposite corner, 6 cm away from the close edges, and mice reexplored for 10 min. Exploration was defined as for the NOR test. The discrimination ratio was calculated as $(time^{Cd} - time^{Cs})/(time^{Cd} + time^{Cs})$, where $time^{Cd}$ and $time^{Cs}$ refer to the time mice explored displaced and stationary objects, respectively, in phase 2.

Three-chamber test

The test was designed in accordance with previous studies with modifications (53). The arena was a white acrylic box (width × depth × height, 60 cm × 40 cm × 25 cm) that was divided into three equal-sized chambers (width × depth × height, 40 cm × 20 cm × 25 cm; Fig. S3C) by two acrylic partitions in which there was an opening (6 cm × 6 cm) located at the central bottom. Two metal grid cups (8 cm × 8 cm × 11 cm) were placed at the center, close to the wall of the two side chambers, and fixed by a water bottle placed above each cup. In the habituation session, all the mice explored the empty arena set with two empty cups. On the test day, in phase 1 (habituation), the mice were habituated to the arena. Then, in phase 2 (sociability test), a stranger mouse (S1) was placed inside a cup, and an object was placed inside the other cup. The subject mice were then placed in the middle chamber and allowed to explore the whole arena freely. Finally, in phase 3 (the social novelty test), the mice reexplored the arena in which the object was replaced by another stranger mouse (S2). Each phase lasted for 10 min. There was no retention time between phases. Both of the stranger mice had never met the subject mouse and had been habituated inside the cup for 10 min/day for 3 days before the test. The following behaviors were counted manually as stimulus exploration: (i) direct interaction with the stimulus (stranger mouse or object) or body parts of the stimulus protruding from the cup, (ii) sniffing the cups with their nose toward the stimulus or sniffing the base of the cup. Standing still near the cups without interaction, sniffing, or climbing to sniff the water bottles were not counted as stimulus exploration.

Metabolic measurements

Pmch-Cre;Slc17a6$^{+/+}$, *Pmch-Cre;Slc17a6*$^{flox/+}$, and *Pmch-Cre;Slc17a6*$^{flox/flox}$ mice were kept separately in single cages beginning at 4 weeks of age. Every 7 days, the mouse body weight and total weekly consumed food pellet weight (CE-2; CLEA Japan) were measured using an accurate scale to a precision of the nearest 0.1 g and followed up until the mice were 15 weeks old.

An ARCO-2000 mass spectrometer (Arco Systems; Kashiwa, Chiba, Japan) was used to indirectly measure the daily energy expenditure. Sixteen-week-old mice were separately kept in each individually sealed chamber (width × depth × height, 14 cm × 14 cm × 12 cm), and the outflow gas from the chamber was controlled and analyzed at the mass flow controller. O_2 and CO_2

concentrations and respiratory quotient (RQ) were determined and calculated (RQ = volume of CO_2 evolved/volume of O_2 consumed). The data were recorded every 5 min. An Actimo-100 N system (Shin, Fukuoka, Japan) was used to record the physical activity (locomotor activity). This system includes a controller connected to an infrared sensor frame (OD width × depth × height, 50 cm × 40 cm × 7 cm; ID width × depth × height: 34 cm × 24 cm × 7 cm) employed to acquire the animal position. These sensors at 20 mm intervals were scanned once every 0.5 s to measure the movement of the mouse. The sealed transparent chamber was placed in the middle of the frame. The total counts were recorded every 30 min. Two systems were controlled by two independent laptops, and up to 8 mice were recorded simultaneously. Mice were habituated to the sealed chamber for 1 day, and the data recorded over the next 2 days were averaged and used in the analysis. Some food pellet pieces were placed inside the chamber, and water was supplied through a chamber-connecting drain. The metabolic schedule and device settings are illustrated in Fig. S4.

Quantification and statistical analysis

Statistical analyses were performed and graphs were generated using GraphPad Prism, version 9 (GraphPad Software, San Diego, CA, USA). Details of the statistical tests are described in Table S1 of the supplementary data and specified in the figure legends. $P < 0.05$ was considered significant.

Acknowledgments

The authors thank S. Nasu, S. Tsukamoto, W. Chen, H. Tang, and R. Lin for their technical assistance and all members of the Department of Neuroscience II at Nagoya University and the Yamanaka Laboratory at CIBR for their continuous support.

Supplementary Material

Supplementary material is available at *PNAS Nexus* online.

Funding

This study was supported by the Beijing Natural Science Foundation (IS23078) and the Chinese Institute for Brain Science, Beijing (CIBR) internal funding to A.Y. This study was also partially supported by the Astellas Foundation for Research on Metabolic Disorders and the Research Foundation for Opto-Science and Technology to A.Y.

Author Contributions

P.X.T. designed, performed the experiments, and analyzed the data. Y.M. and A.Y. contributed to evaluating and interpreting the data for results. Y.A. and K.F.T. performed the experiments and analyzed the data. Y.O. provided some materials for the experiments. A.Y. designed, supervised, and provided funding and resources for the study. D.O. and H.W. co-supervised the study and evaluated the results. P.X.T. wrote the manuscript, Y.M. and A.Y. edited and all authors reviewed.

Data Availability

The authors confirm that the data supporting the findings of this study are available within the article and its supplementary material.

References

1 Bittencourt JC, *et al.* 1992. The melanin-concentrating hormone system of the rat brain: an immuno- and hybridization histochemical characterization. *J Comp Neurol.* 319:218–245.
2 Shimada M, Tritos NA, Lowell BB, Flier JS, Maratos-Flier E. 1998. Mice lacking melanin-concentrating hormone are hypophagic and lean. *Nature*. 396:670–674.
3 Alon T, Friedman JM. 2006. Late-onset leanness in mice with targeted ablation of melanin concentrating hormone neurons. *J Neurosci.* 26:389–397.
4 Kong D, *et al.* 2010. Glucose stimulation of hypothalamic MCH neurons involves KATP channels, is modulated by UCP2, and regulates peripheral glucose homeostasis. *Cell Metab.* 12:545–552.
5 Konadhode RR, *et al.* 2013. Optogenetic stimulation of MCH neurons increases sleep. *J Neurosci.* 33:10257–10263.
6 Jego S, *et al.* 2013. Optogenetic identification of a rapid eye movement sleep modulatory circuit in the hypothalamus. *Nat Neurosci.* 16:1637–1643.
7 Blouin AM, *et al.* 2013. Human hypocretin and melanin concentrating hormone levels are linked to emotion and social interaction. *Nat Commun.* 4:1547.
8 Dilsiz P, *et al.* 2020. MCH neuron activity is sufficient for reward and reinforces feeding. *Neuroendocrinology*. 110:258–270.
9 Adamantidis A, de Lecea L. 2009. A role for melanin-concentrating hormone in learning and memory. *Peptides*. 30: 2066–2070.
10 Izawa S, *et al.* 2019. REM sleep–active MCH neurons are involved in forgetting hippocampus-dependent memories. *Science*. 365: 1308–1313.
11 Monzon ME, *et al.* 1999. Melanin-concentrating hormone (MCH) modifies memory retention in rats. *Peptides*. 20:1517–1519.
12 Varas M, Pérez M, Monzón ME, de Barioglio SR. 2002. Melanin-concentrating hormone, hippocampal nitric oxide levels and memory retention. *Peptides*. 23:2213–2221.
13 Oh ST, *et al.* 2019. Nasal cavity administration of melanin-concentrating hormone improves memory impairment in memory-impaired and Alzheimer's disease mouse models. *Mol Neurobiol.* 56:8076–8086.
14 Ruiz-Viroga V, *et al.* 2023. Acute intrahippocampal administration of melanin-concentrating hormone impairs memory consolidation and decreases the expression of MCHR-1 and TrkB receptors. *Prog Neuropsychopharmacol Biol Psychiatry*. 123:110703.
15 Tan CP, *et al.* 2002. Melanin-concentrating hormone receptor subtypes 1 and 2: species-specific gene expression. *Genomics*. 79:785–792.
16 Adamantidis A, *et al.* 2005. Disrupting the melanin-concentrating hormone receptor 1 in mice leads to cognitive deficits and alterations of NMDA receptor function. *Eur J Neurosci.* 21:2837–2844.
17 Ludwig DS, *et al.* 2001. Melanin-concentrating hormone overexpression in transgenic mice leads to obesity and insulin resistance. *J Clin Invest.* 107:379–386.
18 Izawa S, *et al.* 2022. Melanin-concentrating hormone-producing neurons in the hypothalamus regulate brown adipose tissue and thus contribute to energy expenditure. *J. Physiol.* 600:815–827.
19 Guesdon B, Paradis E, Samson P, Richard D. 2009. Effects of intracerebroventricular and intra-accumbens melanin-concentrating hormone agonism on food intake and energy expenditure. *Am J Physiol Regul Integr Comp Physiol.* 296:R469–R475.
20 Glick M, Segal-Lieberman G, Cohen R, Kronfeld-Schor N. 2009. Chronic MCH infusion causes a decrease in energy expenditure and body temperature, and an increase in serum IGF-1 levels in mice. *Endocrine*. 36:479–485.

21 Pissios P. 2009. Animals models of MCH function and what they can tell us about its role in energy balance. *Peptides*. 30:2040–2044.
22 Cvetkovic V, *et al.* 2004. Characterization of subpopulations of neurons producing melanin-concentrating hormone in the rat ventral diencephalon. *J Neurochem*. 91:911–919.
23 Fort P, *et al.* 2008. The satiety molecule nesfatin-1 is co-expressed with melanin concentrating hormone in tuberal hypothalamic neurons of the rat. *Neuroscience*. 155:174–181.
24 Jiang H, *et al.* 2020. MCH neurons regulate permeability of the median eminence barrier. *Neuron*. 107:306–319.e9.
25 Mickelsen LE, *et al.* 2017. Neurochemical heterogeneity among lateral hypothalamic hypocretin/orexin and melanin-concentrating hormone neurons identified through single-cell gene expression analysis. *eNeuro*. 4:ENEURO.0013-17.2017.
26 Chee MJS, Arrigoni E, Maratos-Flier E. 2015. Melanin-concentrating hormone neurons release glutamate for feedforward inhibition of the lateral septum. *J Neurosci*. 35:3644–3651.
27 Schneeberger M, *et al.* 2018. Functional analysis reveals differential effects of glutamate and MCH neuropeptide in MCH neurons. *Mol Metab*. 13:83–89.
28 Blanco-Centurion C, *et al.* 2018. VGAT and VGLUT2 expression in MCH and orexin neurons in double transgenic reporter mice. *IBRO Rep*. 4:44–49.
29 Sankhe AS, Bordeleau D, Alfonso DIM, Wittman G, Chee MJ. 2023. Loss of glutamatergic signalling from MCH neurons reduced anxiety-like behaviours in novel environments. *J Neuroendocrinol*. 35:e13222.
30 Naganuma F, Bandaru SS, Absi G, Chee MJ, Vetrivelan R. 2019. Melanin-concentrating hormone neurons promote rapid eye movement sleep independent of glutamate release. *Brain Struct Funct*. 224:99–110.
31 Ran FA, *et al.* 2013. Genome engineering using the CRISPR-Cas9 system. *Nat Protoc*. 8:2281–2308.
32 Mohr SE, *et al.* 2016. CRISPR guide RNA design for research applications. *FEBS J*. 283:3232–3238.
33 West DB, *et al.* 2015. A lacZ reporter gene expression atlas for 313 adult KOMP mutant mouse lines. *Genome Res*. 25:598–607.
34 Blackmore DG, Brici D, Walker TL. 2022. Protocol for three alternative paradigms to test spatial learning and memory in mice. *STAR Protoc*. 3:101500.
35 Cruz-Sanchez A, *et al.* 2020. Developmental onset distinguishes three types of spontaneous recognition memory in mice. *Sci Rep*. 10:10612.
36 Inostroza M, Brotons-Mas JR, Laurent F, Cid E, de la Prida LM. 2013. Specific impairment of "what-where-when" episodic-like memory in experimental models of temporal lobe epilepsy. *J Neurosci*. 33:17749–17762.
37 Camats Perna J, Engelmann M. 2015. Recognizing others: Rodent's social memories. In: Wöhr M, Krach S, editors. *Social behavior from rodents to humans*, Current Topics in Behavioral Neurosciences. Springer International Publishing. p. 25–45.
38 Varas MM, Pérez MF, Ramírez OA, de Barioglio SR. 2003. Increased susceptibility to LTP generation and changes in NMDA-NR1 and -NR2B subunits mRNA expression in rat hippocampus after MCH administration. *Peptides*. 24:1403–1411.
39 Bandaru SS, Khanday MA, Ibrahim N, Naganuma F, Vetrivelan R. 2020. Sleep-wake control by melanin-concentrating hormone (MCH) neurons: a review of recent findings. *Curr Neurol Neurosci Rep*. 20:55.
40 Morello GM, *et al.* 2020. High laboratory mouse pre-weaning mortality associated with litter overlap, advanced dam age, small and large litters. *PLoS One*. 15:e0236290.
41 Marsh DJ, *et al.* 2002. Melanin-concentrating hormone 1 receptor-deficient mice are lean, hyperactive, and hyperphagic and have altered metabolism. *Proc Natl Acad Sci U S A*. 99:3240–3245.
42 Chen Y, *et al.* 2002. Targeted disruption of the melanin-concentrating hormone receptor-1 results in hyperphagia and resistance to diet-induced obesity. *Endocrinology*. 143:2469–2477.
43 Karlsson C, *et al.* 2012. Melanin-concentrating hormone receptor 1 (MCH1-R) antagonism: reduced appetite for calories and suppression of addictive-like behaviors. *Pharmacol Biochem Behav*. 102:400–406.
44 Cum M, *et al.* 2024. A systematic review and meta-analysis of how social memory is studied. *Sci Rep*. 14:2221.
45 Chao OY, Nikolaus S, Yang Y-M, Huston JP. 2022. Neuronal circuitry for recognition memory of object and place in rodent models. *Neurosci Biobehav Rev*. 141:104855.
46 Wang X, Zhan Y. 2022. Regulation of social recognition memory in the hippocampal circuits. *Front Neural Circuits*. 16:839931.
47 Rizzi-Wise CA, Wang DV. 2021. Putting together pieces of the lateral septum: multifaceted functions and its neural pathways. *eNeuro*. 8:ENEURO.0315-21.2021.
48 Tong Q, *et al.* 2007. Synaptic glutamate release by ventromedial hypothalamic neurons is part of the neurocircuitry that prevents hypoglycemia. *Cell Metab*. 5:383–393.
49 Swiech L, *et al.* 2015. In vivo interrogation of gene function in the mammalian brain using CRISPR-Cas9. *Nat Biotechnol*. 33:102–106.
50 Platt RJ, *et al.* 2014. CRISPR-Cas9 knockin mice for genome editing and cancer modeling. *Cell*. 159:440–455.
51 Paxinos G, Franklin KBJ. 2001. *The mouse brain in stereotaxic coordinates*. Academic Press.
52 Leger M, *et al.* 2013. Object recognition test in mice. *Nat Protoc*. 8:2531–2537.
53 Rein B, Ma K, Yan Z. 2020. A standardized social preference protocol for measuring social deficits in mouse models of autism. *Nat Protoc*. 15:3464–3477.